Hierarchical Modeling of Polystyrene: From Atomistic to Coarse-Grained Simulations

V. A. Harmandaris, N. P. Adhikari, N. F. A. van der Vegt, and K. Kremer*

Max Planck Institute for Polymer Research, Ackermannweg 10, D-55128, Mainz, Germany

Received March 22, 2006; Revised Manuscript Received May 26, 2006

ABSTRACT: We present a hierarchical approach that combines atomistic and mesoscopic simulations that can generally be applied to vinyl polymers. As a test case, the approach is applied to atactic polystyrene (PS). First, a specific model for atactic PS is chosen. The bonded parameters in the coarse-grained force field, based on data obtained from atomistic simulations of isolated PS dimers, are chosen in a way which allows to differentiate between meso and racemic dyads. This approach in principle allows to study isotactic and syndiotactic melts as well. Nonbonded interactions between coarse-grained beads were chosen as purely repulsive. The proposed mesoscopic model reproduces both the local structure and the chain dimensions properly. An explicit time mapping is performed, based on the atomistic and CG mean-square displacements of short chains, demonstrating an effective speed up of about 3 orders of magnitude compared to brute force atomistic simulations. Finally the equilibrated coarse-grained chains are back mapped onto the atomistic systems. This opens new routes for obtaining well equilibrated high molecular weight polymeric systems and also providing very long dynamic trajectories at the atomistic level for these polymers.

1. Introduction

Molecular simulations provide a very useful tool for understanding the structure−property relations of various materials. Application of these techniques to polymeric materials, however, is not straightforward due to the broad range of length and time scales characterizing them. For example, even a single polymer chain exhibits length scales ranging from the bond length (∼1 Å) to the size of the chain (O(10 nm)) and corresponding time scales ranging from a few femtoseconds for the bond vibrations up to the order of milliseconds or even seconds for the whole chain relaxation. If one deals with entangled systems, the relaxation times can be even much longer.[1−3] Due to this spectrum of characteristic lengths and times involved in polymer systems it is not feasible to take into account all the atomistic degrees of freedom of a polymer chain in a simulation. To increase the length and time scales accessible by simulations, coarse-grained (CG) models have proven to be very efficient.[4]

Coarse-grained molecular models are obtained by lumping groups of chemically connected atoms into "superatoms" and deriving the effective, coarse-grained interaction potentials by averaging over the microscopic details of the atomistic models. The development of coarse-grained particle models for specific polymers is an active research field and various models have been proposed in the literature.[5−15] The degree of coarse-graining, i.e., the number of real atoms represented by one coarse-grained site, or superatom, varies, ranging from a few beads per monomer[5] up to models where many monomers are represented as big blobs[12] or a whole chain is modeled by an elipsoid.[15] The choice of the proper model should be based on the problem considered. If one coarses too many atoms then the mesoscopic model will not be capable of describing, for example properties related to details of the local packing. At the same time, the smaller the number of atomistic particles being coarse-grained, the less the advantages over the detailed atomistic approaches. The typical way for obtaining the effective intramolecular potentials in the coarse-graining representation is by taking into account the atomistic details of the particular polymer. The method first developed by Tschöp et al.,[5] starts from ab initio calculations conducted to determine the full torsional potential of rotatable bonds in the monomeric unit. This information was used to calculate potentials of mean force, associated with distributions of bond lengths and bending and torsional angles of the CG chain representation. Nonbonded excluded volume interactions between CG beads were finally introduced, resulting in a CG force field in which bonded and nonbonded terms are well-separated. We believe that this modeling approach is transferable not only to other polymers but also to more complicated systems (block copolymers, blends, etc.). An improved version of the whole procedure was found to successfully describe structural, dynamical as well as entanglement properties of bisphenol A−polycarbonate (BPA-PC).[14,16,17] In this contribution, a mesoscopic simulation approach, based on the methodology described above, is presented for the modeling of vinyl polymers. As a test case the whole approach is applied to atactic polystyrene (PS).

Polystyrene is one of the most common commercial polymers and probably the most widely studied among all amorphous polymers.[18] In addition to a large amount of experimental data available for PS, molecular modeling techniques have also been applied. Modeling at the atomistic level, using either molecular dynamics (MD)[19−22] or Monte Carlo[23] simulations, has been used to study mainly structural, and some short time local dynamical aspects of bulk atactic PS. Using detailed all-atom or united-atom models it was shown that the simulation results reproduce the experimental data on the density and the structure. However, due to time limitations, in all these atomistic simulation works, only single chain systems[21−22] or very short chains of the order of about 10 monomers have been employed so far.[19−20] Very recently two coarse-grained models of PS have been reported. Milano and Müller-Plathe[9] studied the structural properties of PS by coarse-grained and atomistic models whereas Sun and Faller focused on the dynamics of PS melts.[10] At the same time a coarse-grained model of benzene, based on pretabulated intermolecular potentials optimized in order to describe the thermodynamic properties of the liquid was also

10.1021/ma0606399 CCC: $33.50
Published on Web 08/26/2006

presented.[13] Finally, for related lattice models a procedure for mapping rotational isomeric state (RIS) models onto a coarse-grained representation of a high coordination lattice, which can be applied in vinyl polymers, has also been reported a few years ago by Haliloglou and Mattice.[11]

In the present work, a hierarchical approach that combines atomistic and mesoscopic simulations is developed to study both structure and dynamics of PS. With an eye to the inverse-mapping (reintroduction of atomistic detail) we decided to stay close to the chemically realistic model and map one PS monomer into two effective beads (2:1 model). We also developed a rigorous inverse-mapping scheme that allows to reintroduce chemical details along the CG dynamic trajectory. In combination with an explicit mapping of the time unit in the GG simulation (using dynamic quantities obtained in all-atom simulations of short chains), the inverse-mapping scheme allows to obtain long-time all-atom dynamic trajectories of long chain PS melts, as shown previously for BPA-PC.[17]

The paper is organized as follows. First, the atomistic simulations performed in this work are described in the next section. Then, in section 3, the coarse-graining mapping scheme as well as the generation of the mesoscopic bonded and nonbonded interaction potentials are presented. The simulations of the coarse-grained PS melts are described in detail in section 4, whereas in section 5 structural and dynamical results obtained from the coarse-grained simulations are shown. The inverse-mapping scheme is described and tested in section 6. Finally, our findings and conclusions are summarized in section 7.

2. Atomistic Simulations of Polystyrene

For the atomistic modeling of PS we start with the TraPPE united atom model[24] which reproduces the density of PS over a range of temperatures. United atom models, like TraPPE, were previously found to be very successful in predicting several polymeric properties, showing very good agreement with experimental data, especially for the long-time dynamics (self-diffusion) of low molecular weight bulk polymers with a simple chemical structure (such as polyethylene and polybutadiene).[25,26] The main goal of the present work is the development of a hierarchical methodology that includes microscopic (atomistic) and mesoscopic (coarse-grained) models for the study of the dynamic and rheological properties of high molecular weight polystyrene. Irrespective of the fact that we base the construction of the CG model on an underlying united atom model, in a postprocessing stage, using a rigorous back-mapping scheme (see section 6), we are able, if needed, to create well equilibrated all-atom atomistic configurations as well. We should also note here that in principle the whole coarse-graining procedure can be used for any type of model used in the atomistic description.

In the united atom description each PS monomer is described as eight united atom groups. Five different types of united atoms (CH_3, CH_2, CH, C_{aro}, and CH_{aro}) are defined in a PS chain, whose nonbonded interactions are described by pairwise-additive Lennard-Jones potentials of the form

$$V_{LJ}(r) = 4\epsilon\left[\left(\frac{\sigma}{r}\right)^{12} - \left(\frac{\sigma}{r}\right)^{6}\right] \quad (1)$$

with the parameters ϵ and σ obtained from the TraPPE-UA model[24] and shown in Table 1. Parameters for the unlike interactions were determined using the Lorentz−Berthelot mixing rules.[27] $V_{LJ}(r)$ describes all intermolecular site−site interactions as well as intramolecular nonbonded interactions for atoms separated by more than three bonds. A potential cutoff distance of 1 nm is used. Attractive tail corrections were applied to both the energy and pressure using standard analytical expressions that assume a uniform density distribution beyond the cutoff.[28]

Table 1. Atomistic TraPPE[24] Force Field for the Atactic PS System

nonbonded LJ parameters	ϵ (kJ/mol)	σ (Å)
CH_3 (sp^3)	0.8159	3.75
CH_2 (sp^3)	0.3828	3.95
CH (sp^3)	0.0831	4.65
CH_{aro} (aromatic)	0.4197	3.695
C_{aro} (aromatic link)	0.2494	3.70

bonds (rigid)	l_0 (Å)
CH_3-CH_2	1.54
CH_2-CH	1.54
$CH-C_{aro}$	1.51
$CH_{aro}-CH_{aro}$	1.40

bond bending type	k_θ (kJ/mol/rad^2)	θ_0 (deg)
$CH_3-CH-CH_2$	520	112
$CH_1-CH_2-CH_1$	520	114
$C_{aro}-CH_{aro}-CH_{aro}$	1000	120
$CH_{aro}-CH_{aro}-CH_{aro}$	1000	120
$CH_{aro}-CH_{aro}-C_{aro}$	1000	120
$CH_{aro}-C_{aro}-CH$	1000	120

torsion type	c_0 (kJ/mol)	c_1 (kJ/mol)	c_2 (kJ/mol)	c_3 (kJ/mol)
CH_x-$CH-CH_2-CH$	0.0	2.952	−0.567	6.579

improper dihedral	k_ξ (kJ/mol/rad^2)	ξ_0 (deg)
$CH_{aro}-CH_{aro}-CH_{aro}-CH_{aro}$	167.4	0
$C_{aro}-CH_{aro}-CH_{aro}-CH$	167.4	0
$CH-CH_x-CH_y-C_{aro}$	334.8	35.26

All bond lengths were kept rigid using the SHAKE method,[29] using a relative tolerance of 10^{-4}. The equilibrium bond lengths are listed in Table 1. A harmonic potential is used to describe bond angle bending:

$$V_{bending}(\theta) = \frac{1}{2}k_\theta(\theta - \theta_0)^2 \quad (2)$$

where the constants k_θ and θ_0 are also obtained from the TraPPE model. The torsional potentials, used to describe rotations along bonds in the aliphatic backbone have the following functional form

$$V_{torsional}(\phi) = c_0 + c_1[1 + \cos(\phi)] + c_2[1 - \cos(2\phi)] + c_3[1 + \cos(3\phi)] \quad (3)$$

where the trans state corresponds to 180°. The values for the coefficients c_0, c_1, c_2, and c_3 were taken from the literature.[24]

Finally, to keep sets of four atoms in a specific configuration, a set of "improper dihedral-angle interactions" of the following type are used

$$V_{impr}(\xi) = \frac{1}{2}k_\xi(\xi - \xi_0)^2 \quad (4)$$

where ξ is an improper dihedral angle. Values for the constants k_ξ and ξ_0 are taken from the GROMOS force field.[30] We have used improper dihedral potentials to keep the phenyl ring planar as well as to maintain the tetrahedral configuration around the sp^3 hybridized carbon connecting the phenyl ring. The latter is needed because this tetrahedral center is an united-atom CH group that treats only three bonded neighbors explicitly.[30] All the values for the constants of the intramolecular potential (bond bending, torsional, improper dihedral potential) are reported in Table 1.

Table 2. Atomistic Simulated PS Systems Studied in the Present Work

MW (kDa)	no. of chains	temp (K)	av box size (Å)	sim time (ns)
1	45	463	43.14	50
2	32	463	50.01	100
3	27	463	52.00	300

The molecular dynamics package GROMACS[31] was used to perform all the atomistic MD simulations reported in the present study. The different PS amorphous systems that have been simulated are presented in Table 2. All systems were equilibrated in long MD runs such that the end-to-end vector completely decorrelates. Thus, equilibration, of the short PS melts studied in this work, is not of a problem. All atomistic MD simulations have been conducted under isothermal−isobaric (*NPT*) conditions at $P = 1$ atm using the Berendsen thermostat (coupling time 0.1 ps) and barostat (coupling time 2.0 ps).[32] The integration time step was 2 fs whereas the overall simulation time of the production runs ranged from 50 to 300 ns depending on the chain lengths of the systems studied.

3. Coarse Graining Procedure

3.1. Coarse Graining Procedure. We choose a coarse-grained description of polystyrene in which one monomer of a PS chain is mapped onto two effective coarse grained beads (see Figure 1a), i.e., the coarse-graining scheme is a 2:1 model. The CH_2 group of the backbone chain represents one coarse-grained effective bead (type "A") whereas the remaining CH group of the monomer in the backbone and the phenyl ring are mapped to another effective coarse-grained bead (type "B"). The present mapping scheme chosen for two reasons point in the opposite direction, namely; not loosing too many structural details in comparison to the all atom system and at the meantime to be fast enough in order to study the long time dynamics of polymer melts. At the same time, due to the finer nature of the present mapping scheme, it is relatively easy to develop a rigorous procedure for reinserting all the atomistic details into the CG configurations. Furthermore, chain tacticity is captured in our coarse-graining model through the bending and dihedral potentials (see below). A CG model in which the phenyl group would be represented as one coarse-grained side group and the other atoms of the PS monomer as another, whould require a special potential (improper dihedral) in order to keep the stereochemistry fixed. Very recently, a different mapping scheme for the coarse-grained description of PS was proposed by Milano and Müller-Plathe[9] in which one coarse-grained bead corresponds to a PS dyad. In this coarser model the bond stretching and the bond bending potentials were parametrized to describe the corresponding distribution functions in an atomistic melt of short chains. The nonbonded potentials were derived by iterative Boltzmann inversion such as to reproduce the chain packing of the short-chain melt. Even though no dihedral potential was used, the model proved to describe very well the chain dimension of atactic PS. This is not surprising since in atactic PS the average dihedral angle distribution shows almost no structure. However the case of a stereoregular PS, where a fairly structured dihedral angle distribution exists, will probably be different. The CG model presented by us here follows a different philosophy. Our goal is to have a CG model that will be able to predict the structure and the dynamics of PS melts with different tacticities and also to be able to introduce in a postprocessing stage the atomistic detail at the CG configurations (see section 6) as accurately as possible. This is required for cases where information very close to atomistic detail needed (for example in the study of the diffusion of small penetrants in a high molecular weight PS matrix). For these reasons, we choose a less coarse model (2:1).

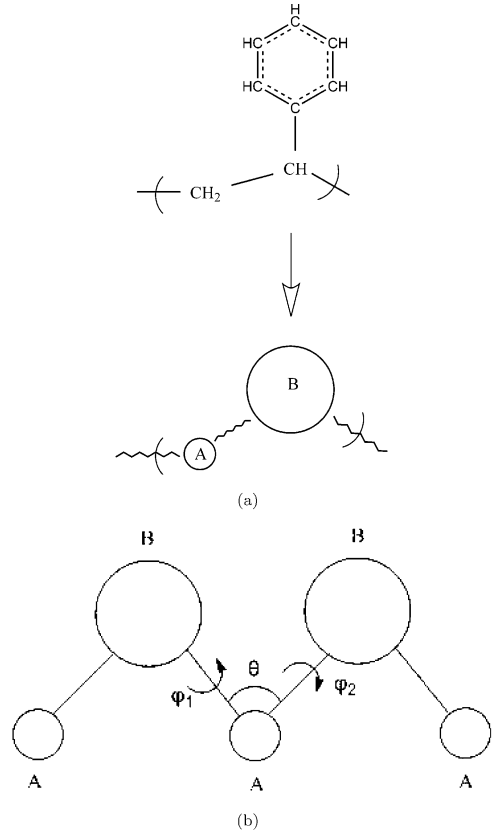

Figure 1. Coarse-graining model of PS: (a) mapping of a PS monomer. (b) a CG PS dimer.

To develop the coarse-grained force field we assume that the total potential energy, U^{CG}, for a coarse grained chain can be separated into two parts i.e., a bonded and a nonbonded part:

$$U^{CG} = \sum U_{\text{bonded}}{}^{CG} + \sum U_{\text{nonbonded}}{}^{CG} \tag{5}$$

The bonded interactions in the above equation are the potentials of mean force of the CG degrees of freedom (bond lengths, angles, dihedrals) and are obtained by sampling distribution functions, P^{CG}, in atomistic simulations of isolated PS dimers. To be able later on to take into account the stereoregularity of the coarse-grained chain model, we generate the distribution functions for all different stereoisomers of the PS dimer. A PS dimer has two stereogenic (chiral) centers which can be either R or S based on the standard IUPAC definition.[33] Therefore, there are four possible PS dimers, i.e., *RS*, *SR*, *RR*, and *SS*. *RS* and *SR* correspond to a meso dyad whereas *RR*, and *SS* are the two enantiomeric forms of the racemic dyad (see Figure 2). In a polymer chain, these dimers are only distinguishable if one defines a direction along the chain contour. First, we performed molecular dynamics simulations, based on the TraPPE model,[24] of the isolated PS dimers and using a Langevin thermostat, which ensures proper equilibration. Then histograms P^{CG} are sampled by collecting a large number of independent conformations for each PS dimer at a given temperature. These probability distribution functions are, in general, unknown functions of the CG bond lengths, r, bending angles, θ, and dihedral angles, ϕ, i.e., $P^{CG}(r, \theta, \phi, T)$. A standard way to proceed,[5] to calculate the CG force field parameters,

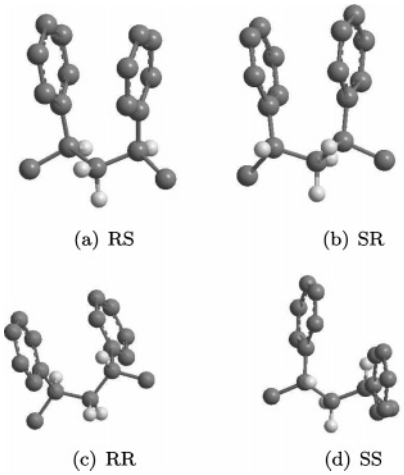

Figure 2. Stereoregular PS sequences used to generate the force field parameters for the CG model: (a) *RS* and (b) *SR* meso dyads; (c) *RR* and (d) *SS* racemic dyads. Hydrogens of phenyl ring and terminal CH_3 groups are omitted for clarity.

is to assume that $P^{CG}(r, \theta, \phi, T)$ factorizes:

$$P^{CG}(r, \theta, \phi, T) = P^{CG}(r, T)\, P^{CG}(\theta, T)\, P^{CG}(\phi, T) \qquad (6)$$

This is of course a drastic simplification and should always be checked and validated. For our model it is thoroughly examined in the next section. Then, having the independent probability distributions, the coarse-grained bonded potentials are given from the inverse Boltzmann relations

$$U^{CG}(r, T) = -k_B T \ln P^{CG}(r, T) + C_r \qquad (7)$$

$$U^{CG}(\theta, T) = -k_B T \ln P^{CG}(\theta, T) + C_\theta \qquad (8)$$

$$U^{CG}(\phi, T) = -k_B T \ln P^{CG}(\phi, T) + C_\phi \qquad (9)$$

where C_r, C_θ, and C_ϕ are irrelevant constants, used to set the minimum of the bond length potential, bond angle potential, and dihedral angle potentials respectively to zero. It should be noted that, in the above expressions, the probability distribution functions for the bond length and bond angle are normalized by taking into account of the corresponding volume elements, namely, r^2 for bond length and $\sin(\theta)$ for the bending angle. Note that by construction the CG potentials contain an entropy contribution and explicit temperature dependence and have to be constructed separately for each temperature T of interest.

Concerning the implementation of the different parts of the bonded potential in the CG representation, the bond stretching potential acts between any two consecutive coarse-grained beads (AB/BA) whereas the bending angle potential acts for the three consecutive coarse-grained beads (ABA and BAB) along a coarse-grained chain. The dihedral angle potential acts for any four consecutive coarse-grained beads along a chain (ABAB or BABA).

Figure 3 presents the bond length distribution of the bonds between beads A and B (AB/BA) and of the distance between two consecutive A beads (AA) for *RS*, *SR*, *RR*, and *SS* PS dimers stereosequences. The AB/BA bond length distribution can be described well with a harmonic type potential fitted to eq 7. The same is also true for the AA distance distribution. Note that although in principle an ABA angle bending potential should be introduced in our model, we choose to instead use a AA distance potential. This choice is justified by the fact that the ABA unit is essentially rigid and the ABA angular distribution function sharply peaked. As we can see from Figure 3, the bond length probability distribution functions, and hence, the bond stretching potentials are equal for all stereoregular sequences.

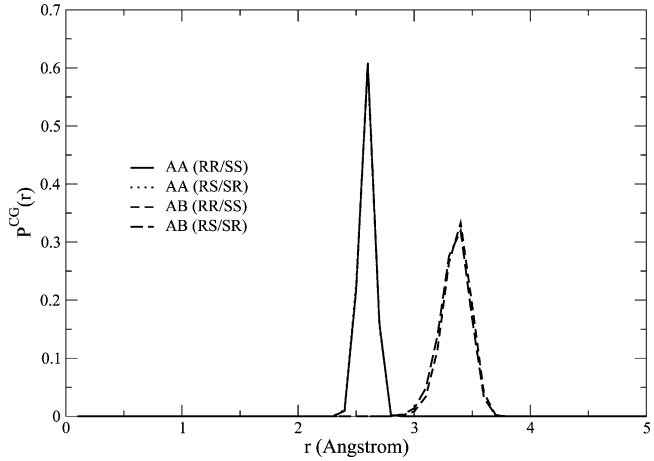

Figure 3. Probability distribution of bond length AB/BA and distance AA for the coarse-grained effective beads. The narrow distribution for the AA distance originates from the only weakly fluctuating bending angle ABA.

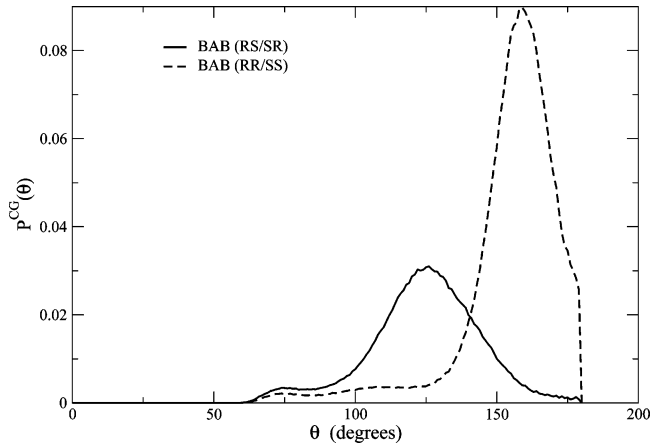

Figure 4. Probability distribution of bending angle BAB for the coarse-grained effective beads at $T = 463$ K.

In Figure 4, the probability distribution function is presented for the bending angle, BAB, of the *RS*, *SR*, *RR*, and *SS* stereosequences, at $T = 463$ K. Obviously the probability distribution of bending angle BAB depends on whether the PS dimer is a meso (*RS*/*SR*) or racemic (*RR*/*SS*) dyad, but it does not depend on whether it is *RS* or *SR*, and *RR* or *SS*, in this mapping scheme. Figure 5, presents the corresponding bending angle potentials of the different sequences obtained using eq 8. For the meso case (full line) the most favorable configuration for the backbone of the chain, in the atomistic representation, is trans/gauche$^-$ (or gauche$^+$/trans). These atomistic configurations correspond to the global minima in the CG bending angle potential (∼118°). The second minimum in the CG bending angle potential (∼70°) is due to the atomistic backbone conformations gauche$^-$/gauche$^+$. For the racemic case (dash line) the most favorable configurations for the atomistic backbone is gauche$^-$/gauche$^+$ which gives the global minima (∼160°) in the CG bending angle (BAB) potential. There is also a shallow second minimum (∼100°) due to the atomistic trans/trans backbone conformations.

Figure 6 shows the probability distribution of dihedral angles (ϕ_1 = ABAB and ϕ_2=BABA) for *RS*, *SR*, *RR*, and *SS* sequences. Note that due to the symmetry of the different PS dyads, their dihedral angles are related. In more detail for the two meso

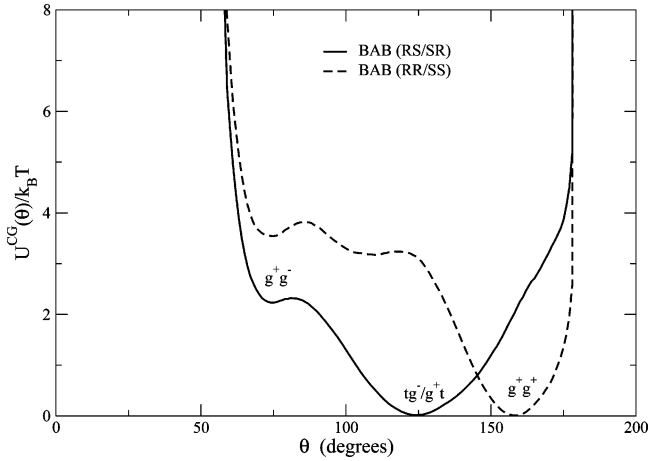

Figure 5. Bending potential for the BAB angle for the meso (*RS*/*SR*) and the racemic (*RR*/*SS*) dyad. The torsional states of the atomistic CH_2-CH and $CH-CH_2$ bonds corresponding to the local minima in the CG bending potential are included: trans (t), gauche$^+$ (g^+), gauche$^-$ (g^-).

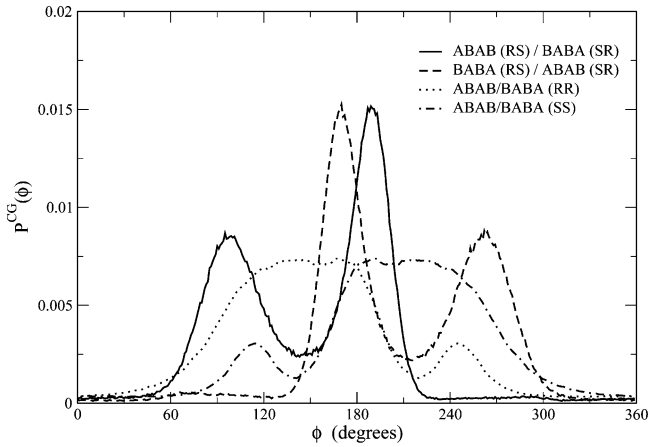

Figure 6. Probability distribution of dihedral angles ABAB and BABA for the coarse-grained effective beads at $T = 463$ K.

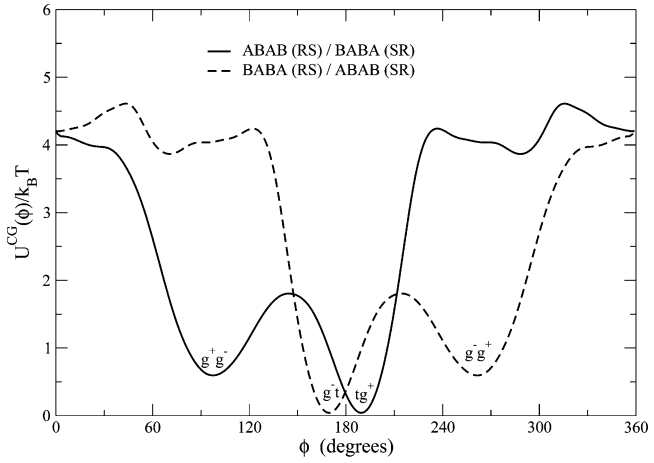

Figure 7. Dihedral potential for the BABA and ABAB angles for *RS* and *SR* PS sequence (meso dyad).

(*RS* and *SR*) dyads, $\phi_1(RS) = \phi_2(SR)$, $\phi_2(RS) = \phi_1(SR)$, and $\phi_1(RS)$ and $\phi_2(RS)$ are mirrored in $\phi = \pi$. For the two racemic (*RR* and *SS*) dyads, $\phi_1(RR) = \phi_2(RR)$, $\phi_1(SS) = \phi_2(SS)$, and $\phi_1(RR)$ and $\phi_1(SS)$ are also mirrored in $\phi = \pi$. The corresponding dihedral potentials for the meso (*RS*/*SR*) dyad are presented in Figure 7. As described above, for the *RS*/*SR* sequence the most favorable configuration for the backbone of the atomistic chain is trans/gauche$^-$ (or gauche$^+$/trans). At the same time due

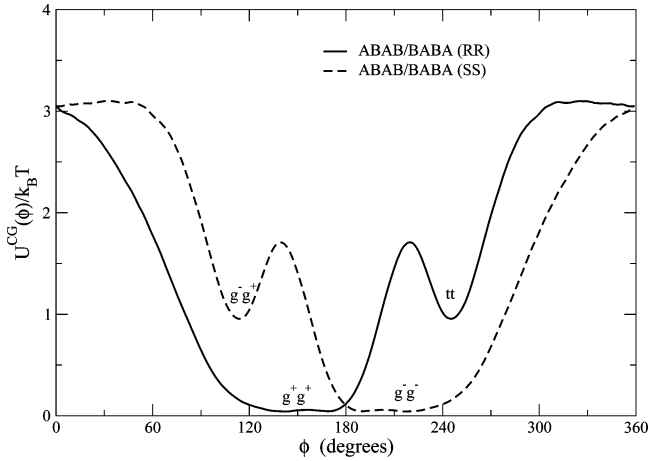

Figure 8. Dihedral potential for the BABA and ABAB angles for (a) *RR* and (b) *SS* PS sequence (racemic dyad).

to steric reasons, when the first four united atoms in the backbone favor the trans (gauche$^+$) configurations, the last four favor the gauche$^-$ (trans). This gives different potentials for the coarse-grained torsions beads (ABAB and BABA) in the *RS*/*SR* sequence. Figure 8 present the dihedral angle potentials for the racemic dyads (*RR*/*SS*). In contrast to *RS*/*SR*, the two dihedral potentials ABAB and BABA for *RR* or *SS* are the same. The global minimum in the dihedral potentials of *RR*/*SS* PS is due to the gauche$^-$/gauche$^+$ conformations of the backbone. The second minima is due to the conformations trans/trans.

Using the procedure described above a complete set of bonded coarse-grained potentials at a specific temperature are obtained. Here we will concentrate on presenting results from a single temperature and therefore data for $T = 463$ K will be presented. In a future work, the temperature dependence of structural and dynamical properties of PS will be investigated. We should also note here that the derived potentials were smoothed by using an averaging procedure so that the forces stay continuous. In this procedure, points in the region of angles which are sampled very rarely (e.g., $\theta \sim 60°$) are smoothed by averaging over a number of n (usually 5−10) neighboring points.

3.2. Correlation of Bending Angle and Dihedral Angle. One of the main assumptions in the development of the coarse-grained model, using the standard methodology described in the previous section, is that all bonded potentials are decoupled and therefore independent bond stretching, bending angle and dihedral angle potentials can be used (see eq 6). However, this is not generally true but in fact strongly depends on the chemical structure of the polymer and also of the specific type of the coarse-grained model. This means that even if there is a perfect matching between the coarse-grained and the atomistic representation for the independent bonded distributions, combinations of different distributions might be very different.

A direct way to check the assumption of the decoupled bonded potentials is by plotting contour plots of energies (or distributions) of combinations of different bonded potentials in the coarse-grained description obtained from the detailed atomistic runs. In the present 2:1 coarse-graining model, it is found that the only interdependence between the bonded mesoscopic potentials is the one between the bending and dihedral coarse-grained angle (θ and ϕ in Figure 1b).

To examine the coupling effect more systematically we choose the racemic sequence for which the effect is more prominent than for the meso case. The interdependence of the bending and the dihedral CG angles is shown in Figure 9, parts a and b, which presents the energy surface plot of the CG

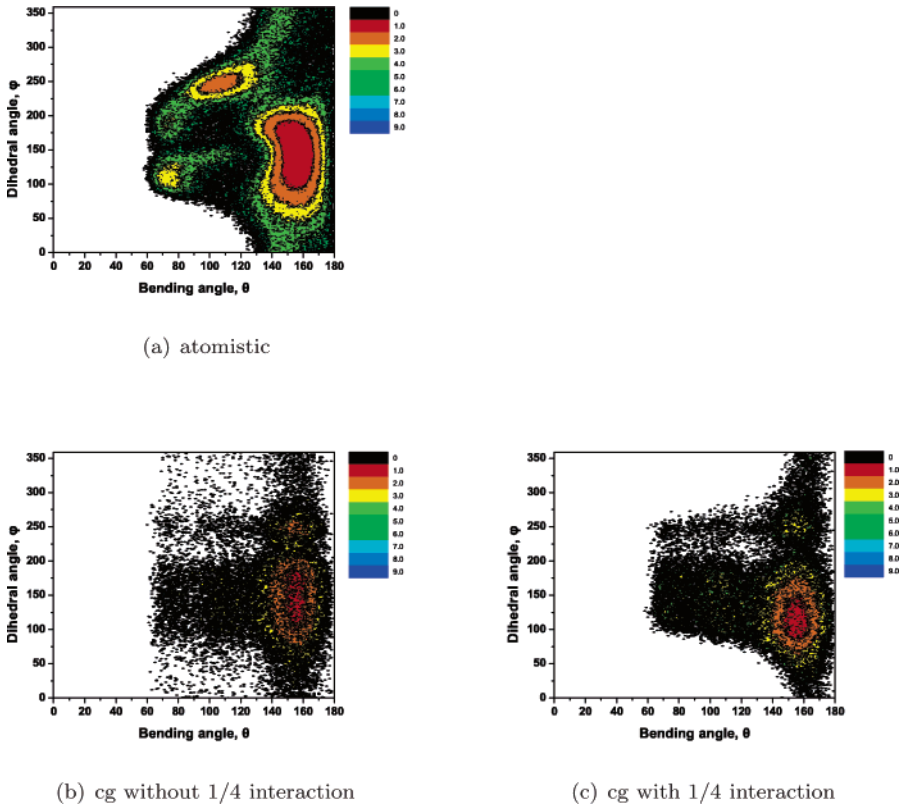

(a) atomistic

(b) cg without 1/4 interaction

(c) cg with 1/4 interaction

Figure 9. ($\theta-\phi$) energy plot in the coarse-grained representation from the atomistic and the CG simulations. The energy units are in k_BT, $T = 463$ K.

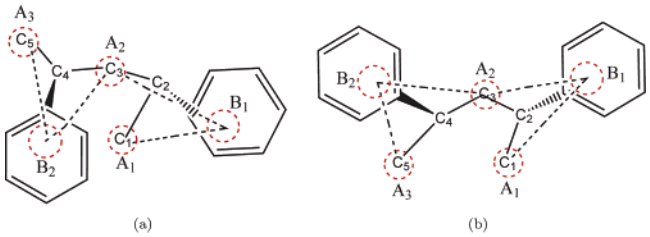

Figure 10. Examples of conformations of PS dimers forbidden in atomistic simulations but still sampled in CG simulations: (a) $\theta(B_1-A_2-B_2) = 90°$, $\phi(B_1-A_2-B_2-A_3) = 300°$ and (b) $\theta(B_1-A_2-B_2) = 160°$, $\phi(B_1-A_2-B_2-A_3) = 240°$.

dihedral angle vs the CG bending angle, i.e., a ($\theta-\phi$) plot, for the *SS* case at $T = 463$ K, obtained from the atomistic (united-atom model) and the coarse-grained simulations of the isolated PS dimers, respectively. If θ and ϕ were uncorrelated one would expect for each ϕ to span the same range of θ values and also for each θ the same range of ϕ. From Figure 9a, it can be seen that this is not the case. The comparison with the coarse-grained simulations, Figure 9b, shows directly similarities but also some significant deviations. In both runs the area of bending and dihedral angles sampled is the same (i.e., bending angle from 60 to 180° and dihedral angle from 0 to 360°) and also the most favorable ($\theta-\phi$) conformations (i.e., $\theta = 155°$ and $\phi = 150°$) are exactly the same. At the same time, there are also some clear differences, the most important of which is that in the mesoscopic runs some conformations (e.g., $\theta = 80°$ and $\phi = 250°$), not allowed in the atomistic simulations, are sampled.

To analyze this problem further, we are identifying these conformations that correspond to the different parts of the atomistic ($\theta-\phi$) plot (Figure 9a), which are not allowed but are still sampled using the CG potential (Figure 9b). In Figure 10, two such typical conformations are presented. The atomistic representation (united atom groups, C_i, and phenyl groups) is shown with the full lines, whereas dashed lines represent the mesoscopic one (coarse-grained A_i and B_i beads). The θ angle plotted in Figure 9 is the $B_1A_2B_2$ one whereas the dihedral ϕ is the $B_1A_2B_2A_3$ angle. The first conformation shown in Figure 10a corresponds to a combination ($\theta = 90°$, $\phi = 300°$), which is entirely forbidden in the atomistic runs due to the excluded volume interaction between atom C_1 and the phenyl group, but allowed in the coarse-grained simulations since this is a (coarse-grained) 1−4 interaction which is described only by a dihedral potential. Similar types of conformations are those that correspond to the lower part of the ($\theta-\phi$) plot, i.e., $\theta = 100°$, $\phi = 50°$. It is important to exclude such conformations also from the coarse-grained simulations, since they are unphysical and an artifact of the decoupling ansatz. A direct way to achieve this is by introducing an additional 1−4 repulsive interaction between the CG beads, which got essentially lost due to the decoupling ansatz. The ($\theta-\phi$) plot from the coarse-grained simulations using this additional interaction, is presented in Figure 9c. Obviously there is a better agreement with the atomistic runs (Figure 9a) mainly in the parts of the graph discussed above. At the same time all the other bonded distributions are exactly the same as without the additional 1−4 repulsive interaction. Therefore, for the CG simulations performed in this work, we take into account the 1−4, nonbonded interaction potential. The parameters of this 1−4 repulsive potential are the same as those used in the other nonbonded interactions of our model (see section 3.3).

The second conformation shown in Figure 10b corresponds to $\theta = 160°$ and $\phi = 240°$. For this ($\theta-\phi$) combination, both, the bending and torsion CG angles are in a (local) minimum of the corresponding potential (cf. Figures 5 and 8). By comparison of Figures 5 and 8, the conflict with the atomistically permitted structure is clear: $\theta = 160°$ corresponds to an atomistic combination g^+g^+ for the torsion angles while $\phi = 240°$ to

another *tt* combinations of atomistic torsions. In the atomistic structure, this ($\theta-\phi$) combination is highly unlikely due to a cis conformation of the atomistic torsion $C_1-C_2-C_3-C_4$. This conformer occurs in the CG distribution because rotation of CG bead A_1 along the CG bond A_2-B_1, while keeping the CG angle B_1-A_2-B_2 fixed in its global minimum ($\theta = 160°$), is permitted. From the underlying chemical structure of the PS dimer, shown in Figure 10b it is clear that the rotation along CG bond A_2-B_1 (involving CG bead C_1) cannot happen independent of moving also CG bead B_1 (and thus changing the angle θ) because A_1 and B_1 are chemically connected through the tetrahedral center C_2. This explain the shift of the second minimum in the atomistic plot, Figure 9a), (i.e., $\theta = 100°$ and $\phi = 250°$) to higher bending angles (i.e., $\theta = 160°$ and $\phi = 250°$) in the CG description.

This example clearly illustrates pitfalls one may encounter in developing CG force fields for models that lump typically around 10 atoms in one superatom. These aspects are usually not discussed in the derivation of CG models, and also illustrate the maximum detail that can be described with the coarse-grained models. In principle one aims to design a CG model that would not show any ($r-\theta-\phi$) interdependencies. However it seems that the direct, and probably the only, way to take properly into account of correlations is by introducing a coupled potential $U(\theta,\phi)$, potential, which in principle can be obtained numerically using all the data of Figure 9a. The disadvantage of such a many-body potential is that it is more costly, decreasing the efficiency of the coarse-grained simulations without giving any advantage for the study of global structural and dynamical properties (see below). The coarse-graining procedure requires a compromise between a choice of mapping, which provides distribution functions as uncorrelated as possible, and on the other hand still contains a close link to the underlying conformations. The present model describes properly the global chain conformations. Moreover, the reinsertion of the atomistic details (inverse mapping, described in section 6) does not lead to unphysical, high energy, states and compares well to experiments. Therefore, we are using here our CG model without any further modifications.

3.3. Nonbonded Interaction Potential. We are calculating independently the nonbonded interaction parameters for type A and type B CG beads. Type A bead is equivalent to a CH_2 united atom group in the atomistic representation, so its σ value can be taken directly from the atomistic one (see Table 1). The σ parameter of the type B beads is obtained by its van der Waals radius, r_{vdw}, which is calculated from the van der Waals radius of a toluene molecule. To perform this calculation one toluene molecule is kept fixed in space while another one is brought at a specific distance r from the first. Then the nonbonded intermolecular potential, using the atomistic force field described in section 2, between the two molecules is calculated by averaging over all possible configurations (orientational angles of rotations) between the two toluenes. Varying the distance between the two molecules, r, the potential of mean force, $U_{PMF}(r, T)$, between center of mass of two toluenes as a function of distance can be calculated:

$$\beta\, U_{PMF}(r, T) = -\ln\langle\exp(-\beta U(r,\Gamma))\rangle_r.$$

In the above relation $U(r,\Gamma)$ is the intermolecular potential for the configuration Γ, in which the distance between the pair of toluene molecules is fixed at r and $\beta = 1/k_BT$. This potential has two different contributions, a repulsive one at small distances and an attractive one at larger distances. In this way, we obtained the van der Waals radius of toluene, $r_{vdwtoluene}$, to be equal to 2.55 Å which compares to the van der Waals radius of 2.85 Å for calculated by Bondi[35] by a group contribution ($-CH_2$ and benzene) method.

Table 3. Coarse Grained PS Systems Studied in the Present Work

MW (kDa)	no. of beads per chain	no. of chains	temp (K)	box size (Å)
1	20	480	463	94.96
2	40	240	463	94.31
3	60	160	463	94.09
5	96	100	463	93.70
10	192	50	463	93.62

The nonbonded interaction potential acts for all the beads from different chains and for the beads which are separated by three or more bonds in the same chain. As discussed in the previous section the 1−4 nonbonded interaction was also taken into account in order to reduce the correlation effect of the bending and dihedral angles. The nonbonded interaction potential is an offset and shifted Lennard-Jones potential:

$$U(r) = 4 \times \epsilon[(\sigma/(r - (r_{ij})))^{12} - (\sigma/(r - (r_{ij})))^6 + {}^1/_4] \quad (10)$$

In the above equation σ is the average of $\sigma_{toluene}$ and σ_{CH_3}, where $\sigma_{toluene}$ is calculated by the van der Waals radius of toluene, assuming that the packing diameter of the molecule ($= 2 \times r_{vdwtoluene}$) is given by the value of r at the potential minimum ($= 2^{1/6}\sigma_{toluene}$), i.e., $\sigma_{toluene} = (2 \times r_{vdwtoluene})/2^{1/6}$. The shift $r_{ij} = \delta r_i + \delta r_j$ allows us to take into account of the different van der Waals volumes of the two mapped groups, i.e., $\delta r_i = \sigma - \sigma_i$ and $\delta r_j = \sigma - \sigma_j$.[5] The strength of the potential is scaled with the temperature, i.e., $\epsilon = k_BT$ whereas the cutoff of the interaction potential is $r_{ij} + 2^{1/6}\sigma$.

4. Simulation of Coarse-Grained PS Melt

The bonded and nonbonded mesoscopic force field, described in the previous section, are used for the coarse graining simulations of atactic PS. The systems we studied are presented in Table 3.

4.1. Generation and Prepacking of the Coarse-Grained PS Chains. The chains are generated by a nonreversal random walk (NRRW) MC algorithm[34] such that all the bond lengths (between consecutive A and B beads as well as nearest A beads) of the CG chains follow the corresponding harmonic probability distributions. The angle at type A bead and the dihedral angles follow the corresponding CG distributions. Further, the 1−5 nonbonded interaction (pentane effect) is also taken into account to generate the initial configuration of the chains. We create an atactic PS melt system with a random end-to-end distribution for the low MW systems (up to 5 kDa). For the higher 10 kDa system, to improve the starting configurations of the high molecular weight systems, only those initial random walks which satisfy an additional condition, i.e., $R^2(N) = C_\infty^{CG} N b^2 \pm 0.15\%$, are accepted (because we have only 50 chains in the simulation box). In this expression, N is the number of beads along the backbone of a chain, i.e., $N = 2n$ with n the number of monomers, $R^2(N)$ is the square distance between monomers separated by N beads and b is the average bond length in the CG model, $b = 3.4$ Å. C_∞^{CG} is the characteristic ratio in the CG description calculated by the experimental value of C_∞ (for PS C_∞ is equal to 9.85[36] at 300 K) corrected for the temperature difference (for PS $d(\ln C_\infty)/d(\ln T) = -0.9 \times 10^{-3}$ [36], so at $T = 463$ K, $C_\infty = 8.5$) and by the bond length b. Using this condition, we chose only those configurations with $C_\infty N b^2$ close to the mean value. This ensures that the internal distances at the time of generation of the polymers chain follow proper distributions for large N.

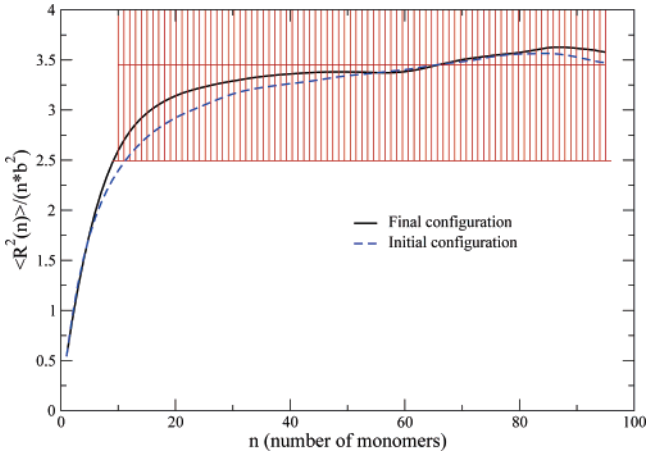

Figure 11. Internal distance distribution for the initial configuration and after equilibration (run of about $10^4\tau$) of a typical system (number of monomers = 96).

The coarse-grained chains are randomly placed in the simulation cubic box. The size of the box is fixed such that the density of PS melt is equal to that of the experimental density at the temperature studied. The coarse-grained PS configurations, generated as described above, have very large local density fluctuations. To decrease the density fluctuations, we perform a zero temperature Monte Carlo simulation in which two different moves (translation or rotation of a chain) are introduced. In this step, we do not change the single chain statistics which by construction have proper internal distances. Details of these MC algorithm can be found elsewhere.[34] The density fluctuation is defined as $\langle \text{nbours}^2 \rangle - \langle \text{nbours} \rangle^2$ where nbours is the number of neighbors of the bead i within a radius of d (d = 0.6Å). Only those moves which decrease the density fluctuations are accepted which helps to reduce the density fluctuations significantly.

4.2. Equilibration of the Coarse-Grained PS Melt. Using the nonbonded and the bonded interactions described in section 3, MD simulations of the coarse-grained PS system are performed using the ESPResSO package.[37] The initially generated chains were strongly overlapping which gives divergent excluded volume interactions. To reduce this effect the intermolecular interaction potential is introduced slowly. To control the temperature in the system we are also using the Langevin thermostat, with friction coefficient $\Gamma = 1.0\tau^{-1}$. Once the overlap is disappeared we introduced full nonbonded interaction potentials to perform the MD simulations. One way to check whether the strong initial overlaps cause undesired conformational changes during the equilibration process is to analyze the internal distances of the chains.[34] Figure 11 presents the internal distances of the chains (after a short run of about 10000 τ), which shows no overshooting at the relatively small distances. The time step used in the MD simulations was $\Delta t = 0.008\ \tau$. We perform MD simulations for times $\sim 10^4$ to $5 \times 10^4\ \tau$ depending upon the system size. We should also state here that in order to use a larger time step the masses of the two different beads were chosen identical; i.e., we assume that the mass of a monomer is uniformly distributed among the two beads. The effect of this assumption on the dynamics, especially at lower temperatures, will be the subject of a future work.

5. Results

We first study the structural results of our mesoscopic simulations. Figure 12 presents the mean squared radius of gyration as a function of number of monomers, $R_G(n)$. It can

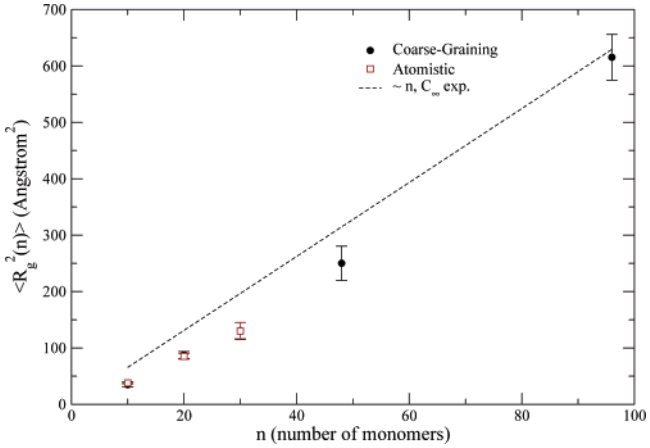

Figure 12. Mean squared radius of gyration as a function of number of monomers in a chain (T = 463 K).

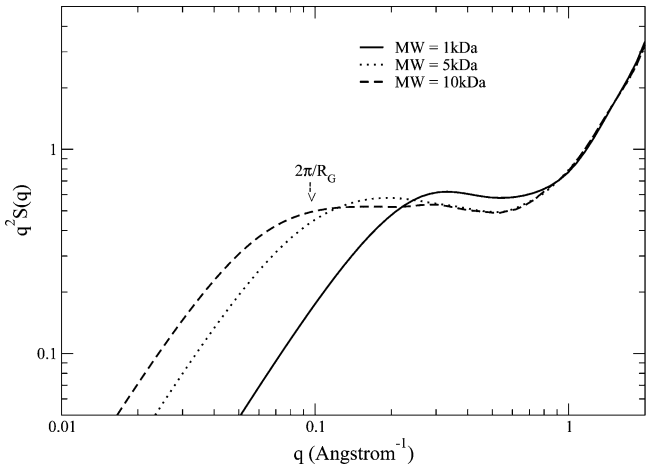

Figure 13. Kratky plot for different PS chain lengths.

be seen that as the length of the PS melt is increasing $R_G(n)$ approaching the value predicted by the random coil hypothesis (linear n dependence, dash line) using the experimental value of C_∞.[36] Results obtained for the short PS chains (up to 30 monomers) from the long atomistic MD simulations (up to 0.3 μs) are, as expected, in excellent agreement with that from the coarse-grained simulations. The reproduction of the radius of gyration of atactic PS from our CG model validates the procedure used to obtain the bonded mesoscopic potentials. In addition, due to the proper dihedral potentials used, it would be expected that with our CG model it would be possible to reproduce the structural properties not only of the atactic-PS, but also the fully isotactic or syndiotactic one. However, the effect of the tacticity on the structural and dynamical properties of PS will be subject to future work.

A standard way to examine the structure of a polymeric chain at all distances is through the static structure factor $S(q)$. Figure 13 presents the standard Kratky plot for 1, 5, and 10 kDa systems at temperature 463 K. In such a plot three different q regimes can be distinguished. The first one is the high q regime ($q \gg 2\pi/b$ with b the bond length, b = 3.4Å) which corresponds to small lengths and where as expected, all the different PS melts have the same structure, i.e., the same $S(q)$. The low q regime ($q \ll 2\pi/R_G$) corresponds to the overall chain dimensions, i.e., the higher the molecular weight the larger the $S(q)$. This is well shown in Figure 13. Finally in the case of a Gaussian chain there is a plateau like regime for $2\pi/R_G < q < 2\pi/b$ (self-similar structure of the chains). In the molecular lengths studied here

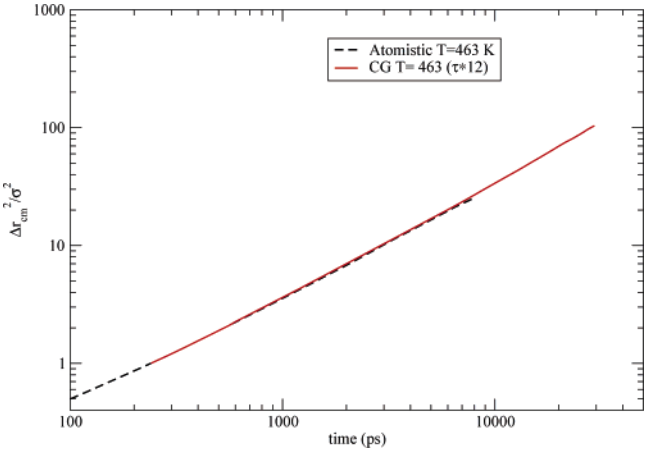

Figure 14. Time mapping of the mesoscopic dynamic simulations using atomistic data for a PS melt (MW = 1 kDa, $T = 463$ K, $\sigma = 4.25$Å).

the plateau like regime is clearly larger for the large molecular weights showing the Gaussian behavior of these chains.

The study of the long time dynamics of atactic PS as a function of temperature and molecular weight is a very important subject and it will be one of the main tasks for detailed investigation in the near future. Here, to give a feeling of the dynamics of PS as predicted from the CG simulations, we are reporting preliminary results about the validation of the CG model. In coarse-graining simulations the time unit (τ) is not known in real units. One way to map the time (τ) is to equate any dynamical quantity like the diffusion coefficient or the viscosity of the coarse-graining model to the one obtained either from detailed atomistic MD runs or to the experimental values. An alternative way is to map directly the mean squared displacement of chain center of mass (or of the monomers) in atomistic simulations and coarse-graining simulations by a proper time scaling of the CG data. The rescaled factor determines the real unit to which one τ corresponds. We follow the last method by using the data of the long atomistic simulations (a few hundrends of nanoseconds) of the short PS oligomers. Figure 14 shows the time mapping for the 1 kDa system at temperature 463 K. We should also state here that due to the small size of the atomistic systems only data up to few ns, shown in the figure, have an error bar below 5%. The rescaled factor, to bring the two curves on top of each other, gives us the CG time unit, which in this case (1 kDa, $T = 463$ K) is

$$1\tau = 12 \text{ ps}$$

It is remarkable that both curves follow exactly each other for distances above only $1-2\ \sigma^2$ and for times above a few hundrends of ps. The possibility to describe accurately the motion of PS chain at such small length and short time scales is one of the advantages of the present CG model and it will be used in the future. We should also note that the time mapping is of course the same, if instead of the chain center of mass displacement, monomer mean-square displacements are used.

Another important aspect of the present CG model is its dynamical efficiency. A time unit τ of 12 ps results in a time step for the integration of equations of motion of ~100 fs. This is about 50 times larger than a typical time step used in the united-atom MD simulations and 100 times larger than typical all-atom atomistic simulations. Taken also into account the smaller number of beads describing a PS chain (2 beads per monomer comparing with 8 in the united-atom and 16 in the all-atom description), the overall efficiency of the model, or the speed-up that can be achieved, is at least ~200 and ~1600 compared with united-atom and all-atom MD simulations, respectively. The actual speed-up is even larger because of the simpler and shorter range nonbonded CG interaction potential, compared with the atomistic one. In addition, as described in details in the next section, in the mesoscopic description it is rather easy to obtain well equilibrated chains of high molecular weight. This is especially important, since for PS this is the only way at the moment.

6. Reinsertion of the Atomistic Detail

As it was also discussed in the Introduction, one of the main goals of the present hierarchical study is to develop a consistent back-mapping procedure from the coarse-grained representation to the atomistic one. The advantage of this procedure is 2-fold: The first is that, by having a proper scheme for reintroducing atomistic detail, well-equilibrated atomistic configurations of a large molecular weight PS system can be obtained. These configurations can be used directly for studying structural properties or can afterward be used for conducting atomistic simulations and predict polymeric properties for which atomistic detail is important. The second advantage is coming from the fact that with the mesoscopic simulations, long time dynamical trajectories can be obtained.[17] By introducing atomistic detail in these trajectories dynamical properties can be predicted and directly compared with experimental data from scattering (eg. neutron spin−echo or dielectric spectroscopy) or nuclear magnetic resonance (NMR) techniques. Finally a rigorous back-mapping procedure is a clear verification of the ability of our coarse-grained model to preserve the chemical identity of the simulated polymer.

For all the above reasons we follow a systematic procedure for reinserting the atomistic detail into the coarse-grained configurations consisting of the following stages.

(A) First we reconstruct each PS monomer unit from its coarse-grained description. As it was stated above, in the coarse-grained representation each PS monomer is modeled as two spherical beads. The first coarse-grained bead of type A (═ CG1) corresponds to the CH_2 unit of the PS monomer whereas the second, larger coarse-grained bead of type B (═CG2) to the CH unit and to the whole phenyl group. Therefore, from the CG2 bead 7 united atom groups (see Figure 1) should be reconstructed. To do this we follow a minimization method, using a quasi-Newton algorithm,[38] in which every united atom (target atom) is constructed based on the coordinates of three other beads (either of the coarse-grained beads and/or of the united atoms of the same monomer, which are already constructed) and taking into account the average equilibrium ("correct") distances between the target atom and three beads obtained from the atomistic configurations. In more details, first the CH united atom of the first monomer is constructed using the coordinates of three groups (the two coarse-grained beads of this monomer and the CH_2 group (═CG1) of the second monomer) and the distances in the atomistic representation between the CH atom and the three groups. The position of the first atom of the phenyl group, C_{aro}, can be directly obtained since it is placed in a fixed distance along the line connecting CH and CG2 beads. Afterward, the rest CH_{aro} groups of the phenyl group are constructed taking into account the coordinates of the CH and C_{aro} united atoms and also the fact that all the atoms of the phenyl group are in the same plane. As a general remark we should noted here that CG means averaging over microscopic states. Any reinsertion procedure generates a

characteristic micro conformation, which belong to these CG schemes. This means that the above minimization scheme is not unique, i.e., starting slightly differently will lead to slightly different states. However it is capable of constructing a subset of characteristic microstates. The construction of the other monomers continues following a similar procedure until the end of the chain is reached. The other chains are then back-mapped in the same way. Finally it should also be mentioned that by following the procedure described above the tacticity of the PS chain is automatically preserved since it is incorporated in the relative positions of two consecutive type B coarse-grained beads, as it was described in detail in section 3.

(B) One of the main assumptions in the derivation of the CG force field is that the distributions of intramolecular CG degrees of freedom factorize. As was described in detail in section 3, this assumption is not entirely true, in particular the point concerning the decoupling between the bending and the torsional potential. The sampling of the CG simulation of the forbidden region (see Figure 9c), even if just a few conformations are sampled, can have as result the appearance of strong overlap in the reconstruction of the atomistic detail. To treat these overlaps after the reinsertion a total minimization procedure is followed, using a steepest decent scheme[38] where the total energy in the system is minimized. The minimization scheme occurs in multiple stages in which the nonbonded LJ interactions gradually introduced. During this minimization procedure atoms are moving a distance of only 1−2 Å^2.

(C) Finally, to obtain a realistic atomistic trajectory at the appropriate temperature (at which the CG model was parametrized), a short NVT MD run, of about 30 ps, is executed.

Using the back-mapping procedure described above, the obtained atomistic configurations can be used for calculating properties in the atomistic level or to perform long atomistic MD runs in well equilibrated large molecular weight atomistic configurations. It should also be noted here that, according to our knowledge, such equilibrated atomistic configurations do not exist so far for PS. To validate the whole procedure we use the 1 kDa system at 463 K for which there are accurate results from both atomistic MD and coarse-grained dynamic simulations. First long CG runs are performed using the CG potential developed in section 3 in a very large system consisting of 480 chains. Afterward the system was back-mapped using the procedure described above (steps A−C) and which incorporates short MD and energy minimization runs.

As a direct check of the reconstruction procedure the pair distribution functions, $g(r)$, are calculated for the 1 kDa system and compared against the one derived directly from "pure very long" (of the order of 100 ns) atomistic runs in a much smaller system of 45 chains. Results are presented in Figure 15 for the intramolecular distribution function obtained both from the long atomistic runs and also from the very short one after the back-mapping procedure (correlations between bonded atoms are not shown for clarity). The agreement between the two curves is excellent for all length scales providing thus a direct evidence of the applicability of the coarse-grained model to preserve the internal chain structure. Of similar quality are the intermolecular distribution functions. Parts a and b of Figure 16 represent the pair correlation functions of the CH_2-CH_2 groups and of the phenyl−phenyl groups, respectively. Again the excellent agreement of the two curves shows the ability of the coarse-grained mesoscopic description to accurately describe the intermolecular structure. However, we should keep in mind the huge speed-up achieved in the CG simulations. For example the brute force atomistic, UA model, MD run even to such a low MW (=1 kDa) PS, and rather small system (45 chains), needs around 50 days in a Power 4 (1.7 GHz) processor, whereas the CG run is a system more than 10 times larger (480 chains) but needs less than 1 day!

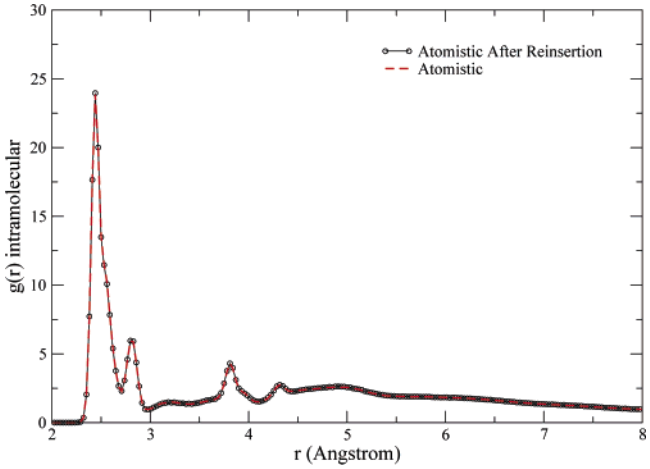

Figure 15. Intramolecular pair distribution function of PS chain from atomistic sinmulations and CG after reinsertion of atomistic detail (MW = 1 kDa, T = 463 K).

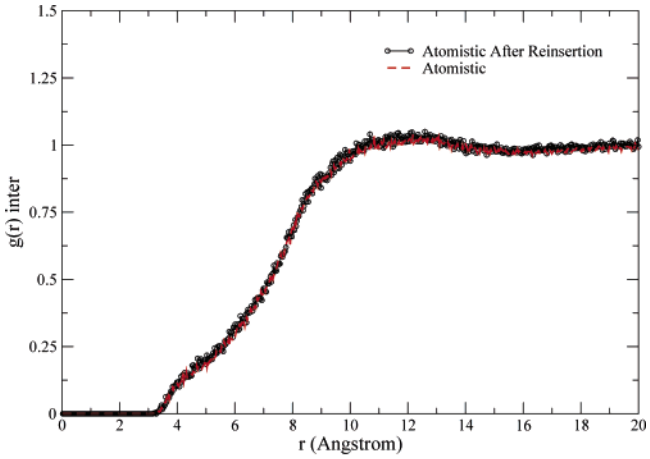

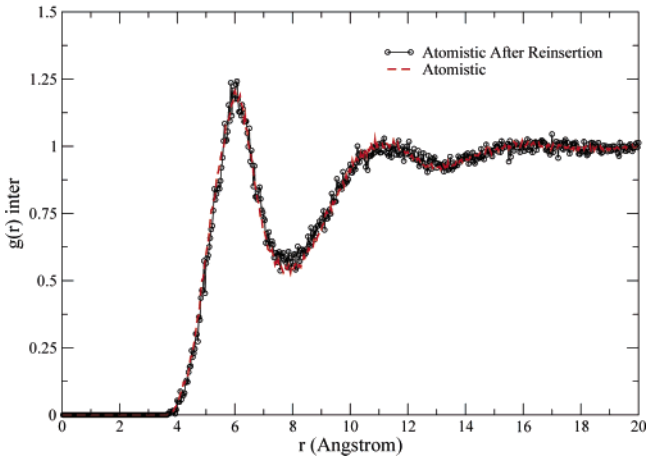

Figure 16. Intermolecular pair distribution function of (a) CH_2-CH_2 groups and (b) phenyl−phenyl rings from atomistic sinmulations and CG after reinsertion of atomistic detail (MW = 1 kDa, T = 463 K).

The atomistic conformations obtained using the reinsertion procedure described above, can now be analyzed and their structure can be compared with experimental data. A typical

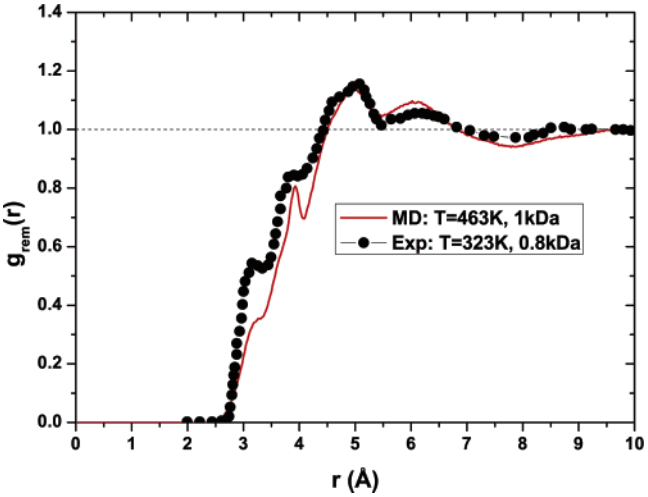

Figure 17. Radial distribution function g_{rem} of PS obtained from CG simulations after reinsertion of atomistic detail and wide-angle X-ray diffraction measurements.

quantity derived in scattering measurements (like X-ray or neutron experiments) is the static structure factor $S(q)$. Fourier inversion of $S(q)$ yields the total radial pair distribution function $g(r)$, which can be also directly calculated from the atomistic configurations. In Figure 17, data about the pair distribution function obtained from wide-angle X-ray diffraction measurements[39] and MD CG simulations, using the reconstruction of the atomistic detail procedure, are presented. In PS the dominant correlations in the total correlation functions are due to the two shortest carbon−carbon distances and also due to the correlations within the phenyl ring. These correlations are also the site−site distances which are almost independent of the molecular conformation due to the very strong bonded interactions. Lodondo et al.[39] in order to compare the chain conformations have excluded these conformationally independent intramolecular correlations (C−C, C−C−C, and between carbons of the phenyl ring) from the experimental data in the level of the scattering function $S(q)$. To compare with these data, we also exclude these correlations in the analysis of the simulation configurations. Of course in the simulation data, we can include these correlations if needed. The remaining part of the total radial distribution function, $g_{rem}(r)$, is shown in Figure 17. In overall there is an excellent agreement between the experiment and the simulation predictions for the whole range of distances, in regard to both the positions and the shapes of the peaks. The differences in the shape of the two short-range correlation peaks are not surprising if one considers that, in the atomistic representation, a united-atom model was used, in which hydrogens are localized on the carbons and therefore gives a much sharper electron-density. The much different temperatures of the two sets of data (temperature of the experimental sample is much below T_g whereas simulations performed in melts) can also result in small differences due to internal stresses present in polymer samples below T_g.

7. Conclusions

In the present work a simulation approach for vinyl polymers, which combines atomistic and mesoscopic simulations, has been presented. As a test case the method has been applied in atactic PS. First, a coarse-grained description of PS was chosen in which each PS monomer is represented as two CG beads (a 2:1 model). Then atomistic MD simulations were conducted on all possible combinations of PS dimer stereosequences, i.e., meso (*RS*/*SR*) and racemic (*RR*/*SS*) and a large number of independent configurations were obtained. Using the atomistic data the effective CG force fields were developed. At the same time a thorough investigation between the coupling of the different bonded mesoscopic potentials has been done. The present CG model is chosen such as that to be capable of preserving the stereochemistry of PS and also being fast enough in order to study polymeric systems of high molecular weight.

The proposed mesoscopic model has been tested along a different number of properties. Structure of short PS chains on the monomeric level (distribution function of bonds, bending and dihedral angles) as well as on the level of the whole chain (internal distances, radius of gyration, end-to-end distance) was found in excellent agreement with the one predicted by very long atomistic MD runs. Also the sizes of the longer chains (radius of gyration, characteristic ratio) are found to be in very good agreement with experimental data. In addition, the generality of the whole procedure, which was previously applied to polycarbonate, should be noted.[5]

An important advantage of the present methodology is the capability to obtain well-equilibrated atomistic configurations of long PS melts. To achieve this, a rigorous approach for reinserting the atomistic detail, that combined minimization and short MD runs, has been developed. The methodology has been successfully tested for short PS chains and the structure was found to be exactly similar to the one obtained directly from very long atomistic MD runs as well as from experimental measurements.

One of the main goals of the present model is to be used in the study of the long time dynamics of high molecular length PS. For this reason a direct investigation of the dynamics in the coarse-grained description has been made by comparing the mesoscopic with the atomistic simulations in the level of mean-square displacements for short PS chains. Future work will consider a detailed study of the time mapping as a function of both molecular length and temperature.

The proposed coarse-grained model can also be used for the study of systems more complicated than the bulk polymer melt. Typical examples can be the study of the diffusion of a penetrant in a polymer matrix, or of block copolymers, blends, etc. In addition, it can be directly incorporated in multiscale methodologies, which include multiple level of simulations, and at the same time both atomistic and mesoscopic descriptions are needed.[40] An example is the study of the long time dynamics of polymers near at solid attractive surfaces[41,42] where an atomistic description needed very close to the surface whereas a mesoscopic description can be used for length scales far from the surface.

Acknowledgment. We are grateful to BASF for financial support. Very fruitful discussions with H. Weiss and C. C. Liew from BASF and with B. Dünweg, D. Andrienko, M. Praprotnik and D. Reith are greatly appreciated. We would like also to thank B. Hess for helping us with the GROMACS program.

References and Notes

(1) *Monte Carlo and Molecular Dynamics Simulations in Polymer Science*; Binder, K., Ed.; Oxford University Press: New York, 1995.
(2) Baschnagel, J.; Binder, K.; Doruker, P.; Gusev, A. A.; Hahn, O.; Kremer, K.; Mattice, W. L.; Müller-Plathe, F.; Murat, M.; Paul, W.; Santos, S.; Suter, U. W.; Tries, V. *Adv. Polym. Sci.* **2000**, *152*, 41.
(3) Kremer, K.; Müller-Plathe, F. *MRS Bull.* **2001**, 205.
(4) Kremer, K. In *Proceedings of the International School of Solid State Physics—34th Course: Computer Simulations in Condensed Matter: from Materials to Chemical Biology*; Binder, K., Ciccoti, G., Eds.; Erice: 2006.
(5) Tschöp, W.; Kremer, K.; Batoulis, J.; Buerger, T.; Hahn, O. *Acta Polym.* **1998**, *49*, 61.

(6) Tschöp, W.; Kremer, K.; Batoulis, J.; Buerger, T.; Hahn, O. *Acta Polym.* **1998**, *49*, 75. (Note that the references 5 and 6 were published with many misprints. Corrections can be obtained from K. Kremer.)
(7) Fukunaga, H.; Takimoto, J.; Doi, M. *J. Chem. Phys.* **2003**, *116*, 8183.
(8) Larson, R. G. *Mol. Phys.* **2004**, *102*, 341.
(9) Milano, G.; Müller-Plathe, F. *J. Phys. Chem. B* **2005**, *109*, 18609.
(10) Sun, Q.; Faller, R. *Macromolecules* **2006**, *39*, 812.
(11) Haliloglou, T.; Mattice, W. L. *J. Chem. Phys.* **1998**, *108*, 6989.
(12) Padding, J.; Briels, W. J. *J. Chem. Phys.* **2002**, *117*, 925.
(13) Zacharopoulos, N.; Vergadou, N.; Theodorou, D. N. *J. Chem. Phys.* **2005**, *122*, 244111.
(14) Abrams, C. F.; Kremer, K. *J. Chem. Phys.* **2001**, *115*, 2776.
(15) Murat, M.; Kremer, K. *J. Chem. Phys.* **1998**, *108*, 4340.
(16) Leon, S.; Van der Vegt, N.; Delle Site. L.; Kremer, K. *Macromolecules* **2005**, *38*, 8078.
(17) Hess, B.; Leon, S.; Van der Vegt, N.; Kremer, K. *Soft Matter* **2006**, *2*, 409.
(18) Ferry, John, D. *Viscoelastic Properties of Polymers*; John Wiley and Sons: New York, 1980.
(19) Tirell, A. R. *Macromolecules* **1992**, *25*, 4605.
(20) Han, J.; Gee, R. H.; Boyd, R. H. *Macromolecules* **1994**, *27*, 7781.
(21) Mondello, M.; Yang, H.; Furuya, H.; Roe, R. *Macromolecules* **1994**, *27*, 3566.
(22) Lyulin, A. V.; Michels, M. A. J. *Macromolecules* **2002**, *35*, 1463.
(23) Rapold, R. F.; Suter, U. W.; Theodorou, D. N. *Macromol. Theory. Simul.* **1994**, *3*, 19.
(24) Wick, C. D.; Martin, M. G.; Siepmann, J. I. *J. Phys. Chem. B* **2000**, *104*, 8008.
(25) Harmandaris, V. A.; Mavrantzas, V. G. In *Simulation Methods for Polymers*; Theodorou, D. N., Kotelyanski, M., Eds.; Marcel Dekker: New York, 2004.
(26) Harmandaris, V. A.; Mavrantzas, V. G.; Theodorou, D. N.; Kröger, M.; Ramirez, J.; Öttinger H. C.; Vlassopoulos, D. *Macromolecules* **2003**, *36*, 1376.
(27) Allen, M. P.; Tildesley, D. J. *Computer Simulation of Liquids*; Claredon Press: Oxford, U.K., 1990.
(28) Frenkel, D.; Smit, B. *Understanding Molecular Simulations*; Elsevier: Amsterdam, 2002.
(29) Ryckaert, J. P.; Ciccoti, G.; Berendsen, H. J. C. *J. Comput. Phys.* **1977**, *101*, 327.
(30) Oostenbrink, C.; Villa, A.; Mark, A. E.; Van Gunsteren, W. F. *J. Comput. Chem.* **2004**, *25*, 1656.
(31) Berendsen, H. J. C.; Van der Spoel, D.; Van Drunen, R. *Comput. Phys. Commun.* **1995**, *91*, 43.
(32) Berendsen, H. J. C.; Postma, J. P. M.; Di Nola, A.; Haak, J. R. *J. Chem. Phys.* **1984**, *81*, 3684.
(33) Clayden, J.; Creeves, N.; Warren, S.; Wothers, P. *Organic Chemistry*; Oxford University Press: New York, 2001.
(34) Auhl, R.; Everaers, R.; Grest, G. S.; Kremer, K.; Plimpton, S. J. *J. Chem. Phys.* **2003**, *119*, 12718.
(35) A. Bondi, *J. Phys. Chem.* **1964**, *68*, 441.
(36) Mark, J.; Ngai, K.; Graessley, W.; Mandelkern, L.; Samulski, E.; Koenig, J.; Wignall, G. *Physical Properties of Polymers*, 3rd ed.; Cambridge University Press: Cambridge, U.K., 2003.
(37) http://www.espresso.mpg.de/; Limbach, H. J.; Arnold, A.; Mann, B. A.; Holm, C. *Comput. Phys. Commun.* **2006**, *174*, 704.
(38) Press: W. H.; Teukovski, S. A.; Vettering, W. T.; Flannery, B. P. *Numerical Recipes*, 2nd ed.; Cambridge University Press: Cambridge, U.K., 1996.
(39) Londono, J. D.; Habenschuss, A.; Curro, J. G.; Rajasekaran, J. J. *J. Polym. Sci., B* **1996**, *34*, 3055.
(40) Praprotnik, M.; Delle Site, L.; Kremer, K. *J. Chem. Phys.* **2005**, *123*, 224106.
(41) Delle Site, L.; Abrams, C. F.; Alavi, A.; Kremer, K. *Phys. Rev. Lett.* **2002**, *89*, 156103.
(42) Harmandaris, V.; Daoulas, K.; Mavrantzas, V. *Macromolecules* **2005**, *38*, 5796.

MA0606399